Bulgarian Chemical Communications, Volume 39, Number 3 (pp. 203–210) 2007

Differential impedance study of solid oxide fuel cell composite cathodes

A. Barbucci[1], M. Viviani[1,2], P. Carpanese[1], D. Vladikova[3]*, Z. Stoynov[3]

[1] *DIChePP, Universita Di Genova, P. Le Kenedi 1, 16129 Genova, Italy*
[2] *CNR, IENI, V. De Marini 6, 16149, Genova, Italy*
[3] *Institute of Electrochemistry and Energy Systems, Bulgarian Academy of Sciences, Acad. G. Bonchev St., Block 10, 1113 Sofia, Bulgaria*

Received June 4, 2006 Revised November 21, 2006

A comparative impedance study of pure LSM $(La_{1-x}Sr_x)_yMnO_{3-\delta}$ with $x = 0.25$ and $y = 0.95$) and composite LSM/YSZ (ZrO_2-8 mol.% Y_2O_3) cathode materials for SOFC is performed. The technique of the Differential Impedance Analysis (DIA), which ensures structural identification without any preliminary hypothesis, is applied to the data analysis. It identifies three steps, determines quantitatively their participation and thus recognizes the rate-limiting step. It is found that the main contribution to the polarization resistance is due to transport limitations. The results obtained by DIA show that the improvement of the LSM/YSZ material for low temperature applications should concern both the ionic and the electronic conductivity.

Key words: LSM cathode material, LSM/YSZ composite cathodes, oxygen reduction, electrochemical impedance spectroscopy, differential impedance analysis.

INTRODUCTION

Solid oxide fuel cells (SOFC) have high electricity conversion degree, superior environmental performance, fuel flexibility and variety of applications. At the moment the challenge is the development of a third generation of planar anode supported SOFC for low operating temperatures (below 700°C). Such conditions increase the cell stability, improve the compatibility of the materials and ensure replacement of the ceramic interconnects by the cheaper metallic alloys.

Requirements to temperature decrease come basically from the reduced conductivity of the active materials. The application of thin electrolyte layers (about 5–10 μm) decreases the electrolyte resistance, which makes the contribution of the cathode/electrolyte polarization critical [1–4].

The increasing demands open new challenges towards the development of improved cathode materials for low temperature SOFC. The investigated materials are composites based on two classical systems for the SOFC: strontium doped lanthanum manganite (LSM), used for cathode, and yttria-stabilized zirconia (YSZ) electrolyte. The LSM material has good electronic conductivity, thermochemical and mechanical stability and compatibility with the electrolyte. The addition of YSZ increases the ionic conductivity of the electrode and the "triple phase boundary" (tpb) contact area, which is distributed in the cathode volume.

The investigation aims at a deeper insight into the complicated conductivity of LSM/YSZ composite by Electrochemical Impedance Spectroscopy (EIS). It is based on comparative study of pure LSM and composite LSM/YSZ. The analysis is performed by the technique of Differential Impedance Analysis (DIA), which ensures structural identification without any preliminary hypothesis for the applied model(s) [5–10]. Our previous DIA studies have shown promising results, recognizing more than one step in the impedance diagrams of the cathode reaction [10].

EXPERIMENTAL

The electrochemical investigations were performed with cathode/electrolyte half-cells using three-electrode configuration [10]. The electrolyte pellets were made by pressing 2.5 g of YSZ (ZrO_2-8 mol.% Y_2O_3, TZ-8YS Tosoh) powder at 12 tons pressure and sintering at 1500°C for 5 hours, resulting in full compact disks 2 cm in diameter and about 2 mm thick.

Cathodes with area 0.23 cm^2 and about 50 μm thick were synthesized from pure LSM and composite LSM/YSZ. The composite electrodes were prepared by wet ball milling of equal volume amounts of YSZ and $(La_{1-x}Sr_x)_yMnO_{3-\delta}$ with $x = 0.25$ and $y = 0.95$ (Praxair) overnight. The mixture was dried and diluted in α-Terpineol (Aldrich) to obtain

* To whom all correspondence should be sent:
E-mail: d.vladikova@bas.bg

a ready painting paste that was thermally treated at 1100°C for 2 hours after depositing it on one side of the electrolyte.

Equi-potential conditions, i.e. homogeneous distribution of current lines were ensured by a layer of highly conducting LSM applied on the working electrode. The ring-shaped reference electrode was painted (Pt ink 6926 Engelhard) on the same side of the electrolyte around the working electrode. Pt counter-electrode of the same size as the working electrode was painted on the opposite side of the electrolyte, facing the cathode. Reference and counter electrodes were then annealed at 900°C for 1 h.

The impedance measurements were carried out in air in the temperature interval 500 to 900°C. A frequency response analyzer Solartron 1260 and an electrochemical interface Solartron 1186 were used for the impedance measurements. They were performed in the frequency range 10^{-1}–10^{6} Hz with amplitude of the a.c. signal 10 mV at equilibrium potential. Each cell was left to stay at the highest temperature for 24 hours before the measurement.

DIA is based on the scanning local analysis [5–10]. It includes a scanning procedure performed using a local estimator called local operating model (LOM) through the whole frequency range, and its parametric identification. The simplest electrochemical equivalent of the applied LOM is a parallel connection of resistance R and capacitance C, extended with the additive term Ad in series. Since in electrochemical systems the resistance of the electrolyte is observed very often at high frequencies, this additive term may be accepted to be a resistance R_{ad} (Fig. 1).

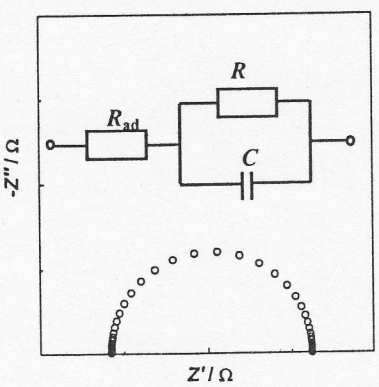

Fig. 1. Local operating model: equivalent circuit and complex plane impedance diagram.

The LOM effective parameters: resistance $\hat{R}$, capacitance $\hat{C}$, time-constant $\hat{T} = \hat{R}\,\hat{C}$ and additive resistance $\hat{R}_{ad}$, are estimated for every measured impedance data set at angular frequency ω_i. The procedure is described in more details in Annex A1. The estimates $\hat{P}_{LOM\,i}$ represent a new experimental data set. Its logarithmic form is used in the next step - the frequency analysis, which provides structural and parametric identification:

$$\lg \hat{\boldsymbol{P}}_{LOM_i}\,[\lg\hat{R}_{ad},\ \lg\hat{R}_i, \lg\hat{C}_i,\ \lg\hat{T}_i] =$$

$$= \boldsymbol{F}(\lg\omega^{-1})_i = \boldsymbol{F}\left(\lg\frac{T_f}{2\pi}\right)_i \qquad (1)$$

where $T_f = f^{-1}$ is the sinusoidal perturbing period.

As T_f represents the time interval of the perturbation, the function $\hat{F}$ is a temporal one and therefore, the analysis is called temporal analysis.

When the LOM corresponds to the nature of the impedance object in a given frequency range, the estimates tend to exhibit constant behaviour in this frequency region. They form a "plateau" in the temporal plot (Fig. 2). In the opposite case frequency dispersion is observed. For Constant Phase Element (CPE) behaviour (Fig. 3a) it is depicted by a linear dependence in the temporal plot (Fig. 3b).

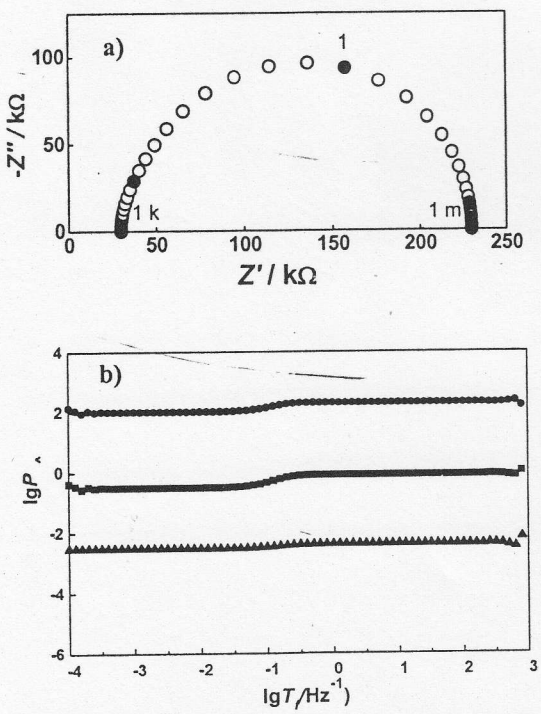

Fig. 2. A model of a Faradaic reaction involving one adsorbed species: (a) complex-plane impedance diagram; (b) temporal plots: $\hat{R}$ - (•), $\hat{C}$ - (▲), $\hat{T}$ - (■).

For the analysis of the dispersion regions in the temporal plots, the so-called Secondary Differential Impedance Analysis is applied [7–10]. It is based on the frequency analysis of the derivatives of the

LOM parameters estimates ($\hat{\delta}_R$, $\hat{\delta}_C$, $\hat{\delta}_T$), called Differential Temporal Analysis (Annex A2).

The following interconnected dependencies represented in the so-called differential temporal plot are valid for CPE behaviour (Fig. 3c):

$$\hat{\delta}_{R_i} = n, \quad \hat{\delta}_{C_i} = 1-n, \quad \hat{\delta}_{T_i} = \hat{\delta}_{R_i} + \hat{\delta}_{C_i} = 1, \quad (2)$$

where n is the CPE exponent.

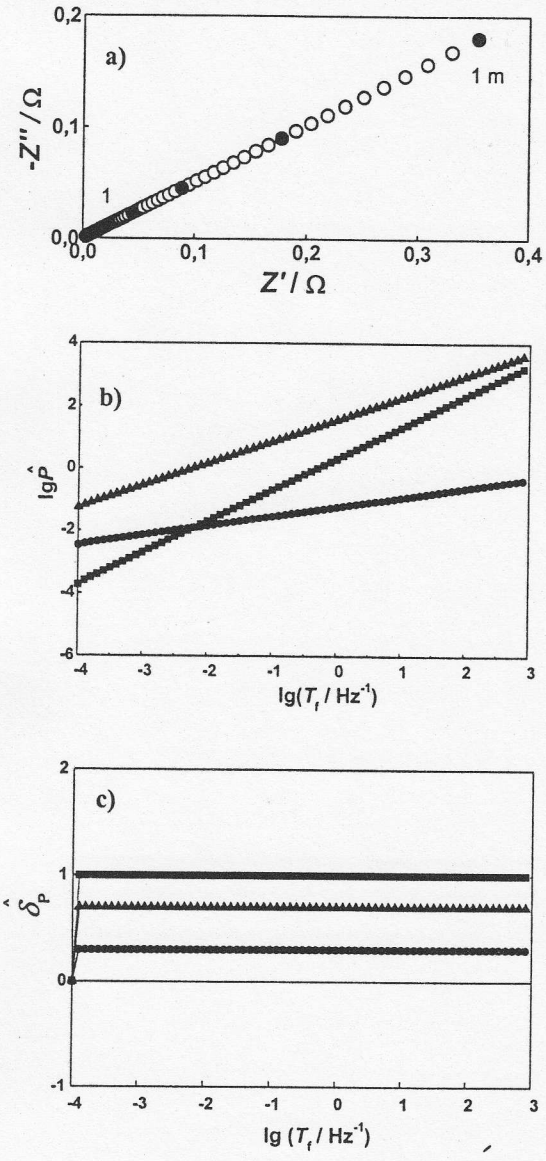

Fig. 3. Constant phase element CPE with $n = 0.25$: (a) complex-plane impedance diagram; (b) temporal plots: $\hat{R}$ - (•), $\hat{C}$ - (▲), $\hat{T}$ - (■); (c) differential temporal plots: $\hat{\delta}_R$ - (•), $\hat{\delta}_C$ - (▲), $\hat{\delta}_T$ - (■).

For more complicated systems a Catalogue with impedance models and their DIA images is applied [8]. In this study, the catalogue was used for the recognition of bounded constant phase element (BCP). This generalized electrochemical element is introduced for impedance description of a homogeneous layer with a finite thickness and bulk conductivity of CPE type [8, 11, 12]. Its impedance is described as:

$$Z_{BCP}(i\omega) = A^{-1}(i\omega)^{-n} \operatorname{th} R_0 A(i\omega)^n, \quad (3)$$

where A, n and R_0 are the structural parameters of the element.

The complex-plane impedance diagram of bounded constant phase element is represented in Fig. 4a. The temporal plots confirm the frequency dispersion of the LOM parameters' estimates over the whole frequency range (Fig. 4b).

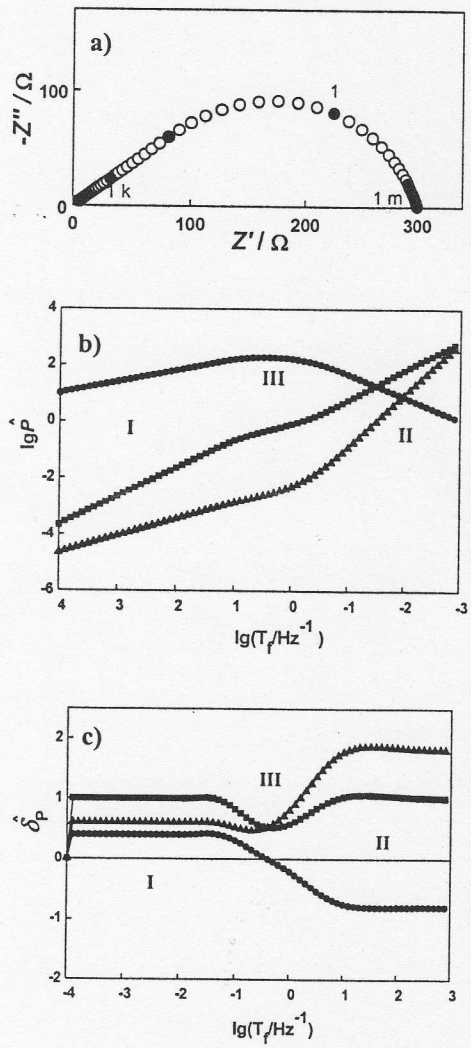

Fig. 4. Bounded constant phase element with $n = 0.4$ and $R_0 = 300\ \Omega$: (a) complex-plane impedance diagram; (b) temporal plots: $\hat{R}$ - (•), $\hat{C}$ - (▲), $\hat{T}$ - (■); (c) differential temporal plots: $\hat{\delta}_R$ - (•), $\hat{\delta}_C$ - (▲), $\hat{\delta}_T$ - (■).

They can be formally divided into two sub-models with a linear behaviour of the dispersion - segment I and segment II in Fig. 4b. The structural identification is based on their Secondary DIA. The two segments are separated by a region of pseudo-

mixing - segment III in Fig. 4b. In the $\hat{R}$ temporal plot it has a shape close to a plateau. Its value corresponds approximately to that of the BCP parameter R_0. The differential temporal analysis of segment I obeys the dependencies given by Eqn. (2). Thus it recognizes a CPE-type of behaviour (Fig. 4c) and ensures identification of the BCP parameter n.

For the structural identification of BCP, however, the Secondary DIA has to be performed also on segment II, since the behaviour of segment I is characteristic also for other sub-models including a CPE component.

The differential temporal analysis of segment II for BCP gives the following dependencies:

$$\hat{\delta}_{Ri} = -2n,\ \hat{\delta}_{Ci} = 1 + 2n,\ .\hat{\delta}_{Ti} = \hat{\delta}_{Ri} + \hat{\delta}_{Ci} = 1 \quad (4)$$

For the example given in Fig. 4 $\hat{\delta}_{Ri} = 0.4$ for Segment I; $\hat{\delta}_{Ri} = -0.8$ for Segment II.

Thus the Differential Temporal Analysis of both segments I and II ensures the structural recognition of BCP.

EXPERIMENTAL RESULTS

Previous impedance results [10, 13] for the cathode reaction on composite materials showed that: (i) the reaction takes place in the volume of the electrode; (ii) the activation energy increases above 700°C.

Since the impedance diagrams are deformed at high temperatures, it was supposed that the observed kink in the Arrhenius plots might be due to inductance (L) error. For its elimination a procedure for L-correction preceded the differential analysis [14]. As it can be seen in Fig. 5, the correction does not eliminate only the inductive tail, but it restores the size, the shape and the position of the observed arc and ensures more precise estimation of the bulk resistance.

Temporal Analysis

The $\hat{R}$, $\hat{C}$ and $\hat{T}$ temporal plots for the pure LSM material show the presence of 3 segments with different frequency behaviour (Fig. 6). The high frequency one (segment I) is frequency independent. It corresponds to a time-constant sub-model, i.e. to an equivalent circuit of resistance and capacitance connected in parallel. It should be noted that there are bigger deviations from the "plateau" behaviour in the $\hat{C}$ and $\hat{T}$ temporal plots for this step. It is supposed that its appearance in the $\hat{R}$ temporal plots is slightly shifted towards lower frequencies.

The segments II and III are frequency dependent. Their analysis needs application of Secondary DIA procedure.

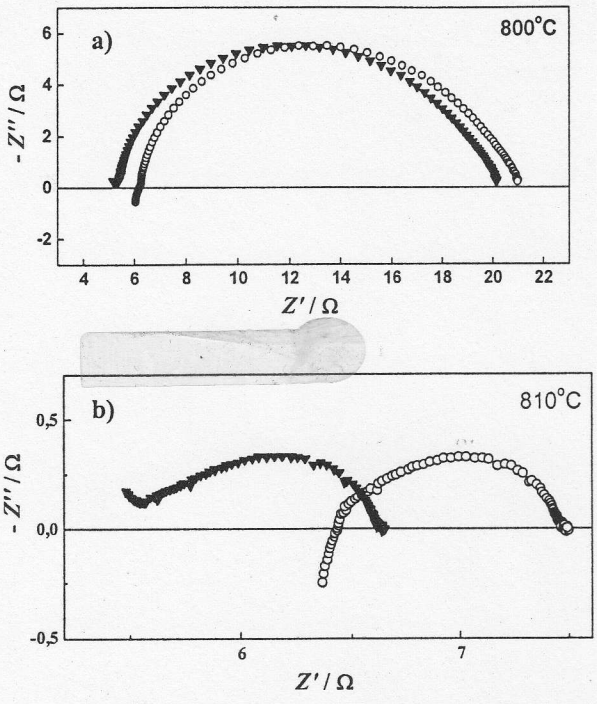

Fig. 5. Impedance diagrams of: a) pure LSM; b) composite LSM/YSZ: Raw data – (○); L- corrected data -(▲).

Segments I and II are observed in the temporal plots of the composite LSM/YSZ electrodes for the whole temperature interval, while the frequency dependent segment III appears at temperatures above 800°C (Figs. 6–8).

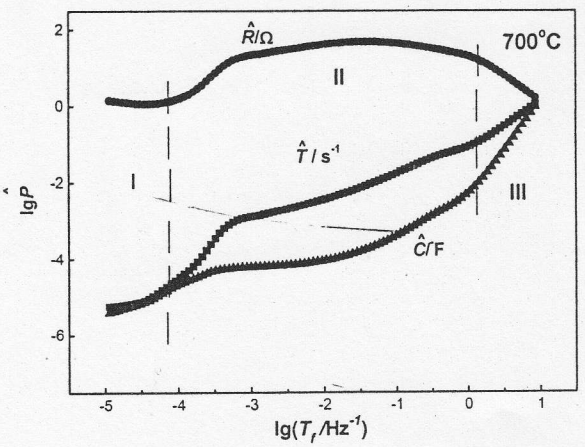

Fig. 6. Temporal plots for pure LSM material.

Differential Temporal Analysis

Step II is well pronounced for both materials in a wide frequency range (3–4 decades) (Figs. 6–8). The temporal analysis shows that its contribution to the cathode resistance is dominant. For its identification a differential temporal analysis is performed for the high frequency IIA and low frequency IIB parts of segment II (Fig. 8).

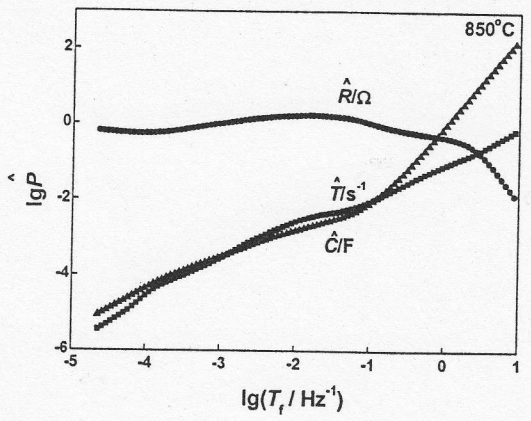

Fig. 7. Temporal plot for composite LSM/YSZ material.

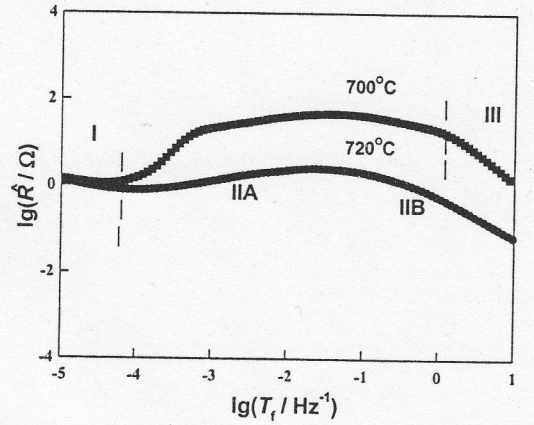

Fig. 8. $\hat{R}$ temporal plots for pure LSM and composite LSM/YSZ.

The obtained results obey the dependences given by Eqns. (2) and (4), which recognize a conductivity with BCP behaviour. The parametric identification is based on the estimation of the structural parameters n and R_0 (Eqn. 3). The exponential term n is determined based on the differential temporal analysis (Eqns. 2 and 4) and the estimate of R_0 – from the maximum between segments IIA and IIB in the $\hat{R}$ temporal plot.

Although Segment II follows the same model for both the pure LSM and the composite LSM/YSZ electrodes, the estimate of the resistance is about one order of magnitude higher for the LSM material. Obviously this step determines basically the cathode polarization resistance and its decrease in the composite samples, since the resistance of step I is of the same order in both materials.

The exponent n, that characterizes the CPE behaviour of the conductivity in step II, is temperature dependent (Fig. 9). Up to 600°C for both materials $n \approx 0.5$. Its value decreases with the increase of the temperature. For the composite electrode $n \approx 0.35$ in the interval 600–650°C. Above this temperature its value is 0.25–0.20. For the pure LSM this change is observed at 750°C.

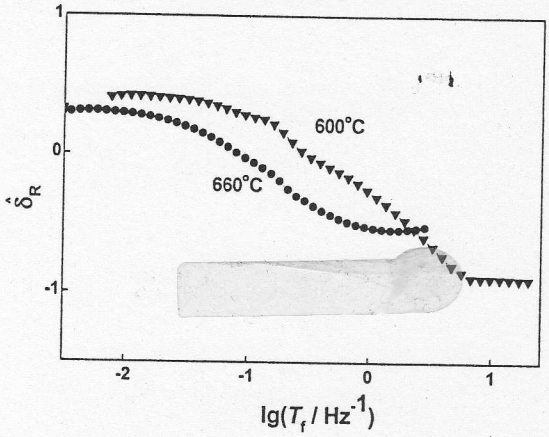

Fig. 9. Differential temporal plot of $\hat{R}$ for composite LSM/YSZ material.

Step III, which appears at low frequencies, has a behaviour strongly dependent on the frequency. It is pronounced in a small frequency range. On this stage of the investigation it cannot be structurally identified. The temporal plots, however, show a strong increase of the effective capacitance, which could be attributed to accumulation of species at the LSM/YSZ surface in both materials. The effective resistance sharply decreases and thus it can not influence the observed values of the polarization resistance.

DISCUSSION

The classical approach for the description of the cathode reaction applies the so-called "triple-phase boundary" concept, which ensures direct involvement of gas phase species at an electrochemical interface [17]. However, to characterize the reaction, it is represented with several individual steps: charge transfer across a two-dimensional interface, adsorption, solid state migration and gas diffusion. This approach is very convenient for impedance studies [18–21].

Recently a non-charge transfer approach, known as ALS model, has been developed for characterization of oxygen reduction on single- and double-phased porous mixed conducting oxygen electrodes [22–25]. It supposes that: (i) the actual interfacial charge-transfer is very fast, provided the interface is not contaminated; (ii) the electrode reaction takes place over a finite distance beyond the electrode/electrolyte interface, which may reach 20 microns, depending on the exchange and diffusion properties of the mixed conductor.

The results obtained by DIA give additional information for the processes that characterize the

polarization resistance of the investigated cathode materials. The technique identifies three steps, determines quantitatively their participation and thus recognizes the rate-limiting stage. The estimation of the effective resistance for steps I and II at different temperatures enables the calculation of their activation energies (Fig. 10).

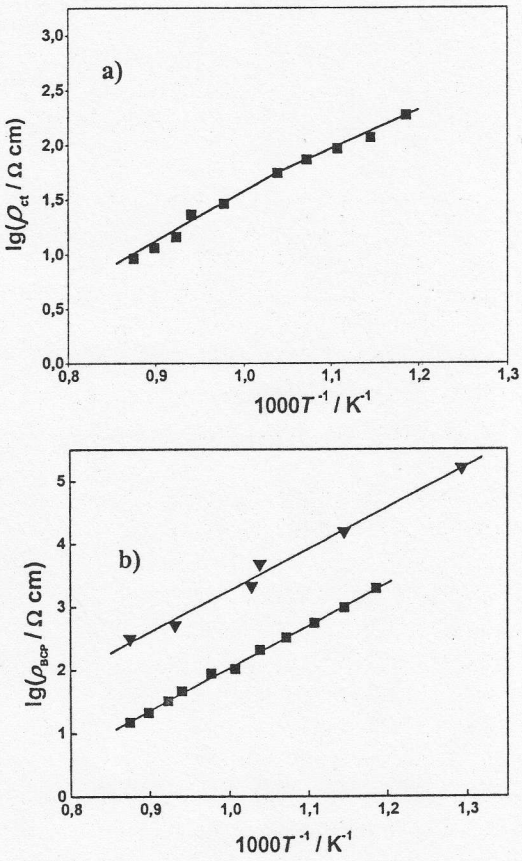

Fig. 10. Arrhenius plots for: a) resistivity of step I; b) resistivity of step II.

Step I. The effective resistance for this step (R_I) is similar for both the pure LSM and the composite LSM/YSZ electrodes (Fig. 8). It decreases with the temperature. The observation of this step in the high frequency region, as well as the low values of its resistance, which are similar for the two electrode materials, suppose a charge transfer process for step I [23–27]. Its activation energy increases from 0.7 eV below 700°C up to 0.9 eV at higher temperatures (Fig. 10a). The results, obtained in this study, confirm the hypothesis of Kilner and co-workers [27] for impediments in the charge transfer at higher temperatures.

Step II. This step has the biggest contribution in the polarization resistance of the two materials. The estimates of R_0 (R_{II}) demonstrate the quantitative differences of the resistance for the pure LSM and the composite LSM/YSZ material, while n is more informative with respect to the mechanism.

In principle bounded constant phase element with n = 0.5 describes diffusion limited conductivity. This situation is observed for both materials at lower temperatures. The decrease of n with the temperature informs for changes in the transport of the species. For $n \leq 0.35$ BCP describes conductivity with restrictions of the host matrix. They decrease with the temperature.

It is interesting to note, that the activation energy of step II for both the pure LSM and the composite material is one and the same – about 1.3 eV in the whole temperature range.

The comparative analysis of the changes in the effective resistance with the temperature for both materials gives very interesting results. In the case of pure LSM the resistance of step II (R_{II}) is strongly dominating for the whole temperature interval, while for the composite electrode this situation is valid only for low temperatures (up to 600°C). Since R_{II} decreases more quickly than R_I, at higher temperatures the two components become comparable (at 700°C $R_{II} \approx 3R_I$).

The improvement of the properties of pure LSM is connected with the increase of the ionic conductivity, which is related to step II. The results obtained by DIA for the composite LSM/YSZ reveal a new moment – they show that the optimization of the material needs improvements both in the ionic and in the electronic conductivity, which could ensure operation at low temperatures.

Although R_{II} for both materials is very different, the activation energies are found to be the same and the conductivities follow one and the same model. This result suggests that the cathode reaction could be improved by optimization of the microstructure.

The results obtained by DIA give novel information about the conductivity of composite LSM/YSZ cathode materials for SOFC and approaches for their improvement.

Acknowledgements: *The authors acknowledge gratefully the support by the European Commission (specific programme "Energy, Environment and Sustainable Development – Part B: Energy program) under contract NNE5/2002/18 "Portable and Emergency Energy Sources" that made possible the international collaboration in this work.*

ANNEX A1

Basics of DIA

The impedance of the LOM is:

$$Z_{LOM}(i\omega) = R + \frac{R}{1+\omega^2T^2} - i\frac{\omega RT}{1+\omega^2T^2}. \quad (A1.1)$$

Since the frequency is known, equation (A1.1) can be presented in a parametric form:

$$\boldsymbol{P}(\mathrm{i}\omega) = \left| \; R + \frac{R}{1+\omega^2 T^2}, \mathrm{i}\frac{\omega RT}{1+\omega^2 T^2} \; \right|, \quad \text{(A1.2)}$$

where $\boldsymbol{P}(\mathrm{i}\omega)$ is the vector of the parameters. The imaginary term can be expressed as an effective inductance. Then (A1.2) takes a more general form:

$$\boldsymbol{P}(\mathrm{i}\omega) = |Re(\omega), \mathrm{i}L_{\mathrm{eff}}(\omega)|. \quad \text{(A1.3)}$$

The derivatives of the real and imaginary components of the impedance are:

$$\frac{\mathrm{d}\,Re(\omega)}{\mathrm{d}\omega} = -R\frac{2\omega T^2}{(1+\omega^2 T^2)^2} \quad \text{(A1.4)}$$

and

$$\frac{\mathrm{d}L_{\mathrm{eff}}(\omega)}{\mathrm{d}\omega} = -RT\frac{2\omega T^2}{(1+\omega^2 T^2)^2}. \quad \text{(A1.5)}$$

The time-constant is derived as:

$$\hat{T}(\omega) = \frac{\mathrm{d}\,L_{\mathrm{eff}}(\omega)}{\mathrm{d}\omega} \Big/ \frac{\mathrm{d}\,Re(\omega)}{\mathrm{d}\omega} = \frac{\mathrm{d}\,L_{\mathrm{eff}}(\omega)}{\mathrm{d}\,R_{\mathrm{eff}}(\omega)} \quad \text{(A1.6)}$$

Then the other parameters are calculated:

$$\hat{R}(\omega) = -\frac{\mathrm{d}\,Re(\omega)}{\mathrm{d}\omega} \cdot \frac{[1+\omega^2 \hat{T}^2(\omega)]^2}{2\omega \hat{T}^2(\omega)}, \quad \text{(A1.7)}$$

$$\hat{R}_{\mathrm{ad}}(\omega) = Re(\omega) - \frac{\hat{R}(\omega)}{1+\omega^2 \hat{T}^2(\omega)}, \quad \textit{(A1.8)}$$

$$\hat{C}(\omega) = \hat{T}(\omega) / \hat{R}(\omega). \quad \text{(A1.9)}$$

ANNEX A2

Secondary DIA

The Secondary Differential Impedance Analysis is performed by differentiation of the logarithmic LOM parameters' estimates (Eqn. 1) with respect to the logarithm of the frequency. It presents their frequency dependence in the form:

$$\hat{\delta}_{P_i} = \left(\frac{\mathrm{d}\lg(\hat{P})}{\mathrm{d}\lg(\omega^{-1})} \right)_i = \boldsymbol{\Phi}(\lg\omega^{-1})_i' = \boldsymbol{\Phi}\left(\lg\frac{T_{\mathrm{f}}}{2\pi} \right)_i = \boldsymbol{\Phi}(\nu)_i, \quad \text{(A.2.1)}$$

where $\nu_i = \lg(\omega^{-1})_i$.

Thus a new set of functions is obtained:

$$\hat{\delta}_{\mathrm{T}i} = \mathrm{d}\lg\hat{T}_i / \mathrm{d}\nu_i = \boldsymbol{\Phi}(\nu_i), \quad \text{(A2.2)}$$

$$\hat{\delta}_{\mathrm{R}i} = \mathrm{d}\lg\hat{R}_i / \mathrm{d}\nu_i = \boldsymbol{\Phi}(\nu_i), \quad \text{(A2.3)}$$

$$\hat{\delta}_{\mathrm{C}i} = \mathrm{d}\lg\hat{C}_i / \mathrm{d}\nu_i = \boldsymbol{\Phi}(\nu_i), \quad \text{(A2.4)}$$

$$\hat{\delta}_{\mathrm{R_{ad}}_i} = \mathrm{d}\lg\hat{R}_{\mathrm{ad}_i} / \mathrm{d}\nu_i = \boldsymbol{\Phi}(\nu_i). \quad \text{(A2.5)}$$

They form a new estimated data set $\boldsymbol{D}$:

$$\boldsymbol{D}(\nu_i, \hat{\delta}_{\mathrm{T}i}, \hat{\delta}_{\mathrm{R}i}, \hat{\delta}_{\mathrm{C}i}, \hat{\delta}_{\mathrm{R_{ad}}_i}). \quad \text{(A2.6)}$$

Since the Secondary Analysis formulated by Eqn. A2.1 describes the differentiation of the temporal functions, it is called Differential Temporal Analysis.

REFERENCES

1. J. T. Vaughey, Xiaoping Wang, J. D. Carter, M. Krumpelt, in: Solid Oxide Fuel Cells (SOFC VI), S. C. Singhal, M. Dokiya (eds.), The Electrochemical Society Proceedings Series, Pennington, NJ, 99/19, 1999, p. 361.
2. Y. Takeda, Y. Sakaki, T. Ichikawa, N. Imanishi, O. Yamamoto, M. Mori, N. Mori, T. Abe, *Solid State Ionics*, **72**, 257 (1994).
3. A. Hammouche, E. J. L. Schouler, M. Henault, *Solid State Ionics*, **28–30**, 205 (1998).
4. A. Barbucci, P. Piccardo, M. P. Carpanese, M. Viviani, in: Portable and Emergency Energy Sources, Z. Stoynov, D. Vladikova (eds.), Marin Drinov Academic Publishing House, Sofia, 2006, p. 329.
5. D. Vladikova, P. Zoltovski, E. Makowska, Z. Stoynov, *Electrochim. Acta*, **47**, 2943 (2002).
6. D. Vladikova, Z. Stoynov, M. Viviani, *J. Europ. Ceram. Soc.*, **24**, 1121 (2004).
7. D. Vladikova, Z. Stoynov, *J. Electroanal. Chem.*, **572**, 377 (2004).
8. Z. Stoynov, D. Vladikova, Differential Impedance Analysis, Marin Drinov Academic Publishing House, Sofia, 2005.
9. D. Vladikova, A. Kilner, S. J. Skinner, G. Raikova, Z. Stoynov, *Electrochim. Acta*, **51**, 161 (2006).
10. A. Barbucci, M. Viviani, P. Carpanese, D. Vladikova, Z. Stoynov, *Electrochim. Acta*, **51**, 1641 (2006).
11. Z. Stoynov, B. Grafov, B. Savova-Stoynova, V. Elkin, Electrochemical Impedance, Nauka, Moscow, 1991 (in Russian).
12. Z. Stoynov, B. Savova-Stoynova, N. V. Stamenova, *Bulg. Chem. Commun.*, **27**, 289 (1994).
13. A. Barbucci, P. Carpanese, G. Cerisola, *Solid State Ionics*, **176**, 1753 (2005).
14. Z. Stoynov, D. Vladikova, in: Portable and Emergency Energy Sources, Z. Stoynov, D. Vladikova (eds.), Marin Drinov Academic Publishing House, Sofia, 2006, p. 383.
15. S. Ikeda, O. Sakurai, K. Uematsu, N. Mizutani, M. Kato, *J. Mater. Sci.*, **20**, 4593 (1985).
16. S. P. S. Badwal, *J. Mater. Sci.*, **19**, 1767 (1984).
17. A. Schmid, *Helv. Chim. Acta*, **1**, 169 (1933).

18. E. Perry Murray, S. A. Barnett, in: Solid Oxide Fuel Cells (SOFC VI), S. C. Singhal, M. Dokiya (eds.), The Electrochemical Society Proc. Series, Pennington, NJ, 99/19, 1999, 369.
19. F. H. van Heuveln, H. J. M. Bouwmeester, *J. Electochem. Soc.*, **144**, 134 (1997).
20. M. Lui, Z. Wu, *Solid State Ionics*, **107**, 105 (1998).
21. B. A. Boukamp, *Solid State Ionics*, **136–137**, 75 (2000).
22. S. B. Adler, J. A. Lane, B. C. H. Steele, *J. Electrochem. Soc.*, **143**, 3554 (1996).
23. S. B. Adler, *Solid State Ionics*, **111**, 125 (1998).
24. S. B. Adler, *Solid State Ionics*, **135**, 603 (2000).
25. B. C. H. Steele, K. M. Hori, S. Uchino, *Solid State Ionics*, **135**, 445 (2000).
26. C. Gabrielli, Identification of Electrochemical Processes by Frequency Response Analysis, Technical Report No 004, Solartron, Farnborough, Hampshire, England, 1980.
27. P. S. Maning, J. D. Sirman, J. A. Kilner, *Solid State Ionics*, **93**, 125 (1997).

ДИФЕРЕНЦИАЛНО ИМПЕДАНСНО ИЗСЛЕДВАНЕ НА КОМПОЗИТНИ КАТОДИ ЗА ТВЪРДОКИСНИ ГОРИВНИ КЛЕТКИ

А. Барбучи[1], М. Вивиани[2], П. Карпанезе[1], Д. Владикова[3]*, З. Стойнов[3]

[1] ОИХП, Университет на Генуа, пл. Кенеди 1, 16129 Генуа, Италия
[2] НСИ, ИЕГП, бул. „Де Марини" № 6, 16149, Генуа, Италия
[3] Институт по електрохимия и енергийни системи, Българска академия на науките, ул. „акад. Г. Бончев" бл. 10, 1113 София

Постъпила на 4 юни 2006 г., Преработена на 21 ноември 2006 г.

(Резюме)

Проведено е сравнително импедансно изследване на катодни материали за твърдокисни горивни клетки (ТОГК) на база чист ЛСМ ($La_{1-x}Sr_x)_y MnO_{3-\delta}$ с $x = 0.25$ и $y = 0.95$) и композитен ЛСМ/ИСЦ (ZrO_2-8 мол.% Y_2O_3). За анализ на данните е използвана техниката на диференциалния импедансен анализ (ДИА), която осигурява структурна идентификация без необходимост от предварителна хипотеза. Идентифицирани са три стъпки, които са охарактеризирани количествено, при което е дефиниран скоростоопределящия стадий. Установено е, че основният дял в поляризационното съпротивление се определя от транспортните ограничения. Получените чрез ДИА резултати показват, че подобряването на материала ЛСМ/ИСЦ за приложение при ниски температури е свързано с намаляване както на йонната, така и на електронната проводимост.